Received: 4 May 2024 | Revised: 11 July 2024 | Accepted: 23 July 2024

DOI: 10.1111/ppl.14463

ORIGINAL RESEARCH

Physiologia Plantarum

Metals and other ligands balance carbon fixation and photorespiration in chloroplasts

Xiaoxiao Shi | Nathan M. Hannon | Arnold J. Bloom

Department of Plant Sciences, University of California at Davis, Davis, CA

Correspondence
Arnold J. Bloom
Email: ajbloom@ucdavis.edu

Funding information
National Science Foundation, Grant/Award Number: CHE-19-04535

Edited by A. Krieger-Liszkay

Abstract

The behavior of many plant enzymes depends on the metals and other ligands to which they are bound. A previous study demonstrated that tobacco Rubisco binds almost equally to magnesium and manganese and rapidly exchanges one metal for the other. The present study characterizes the kinetics of Rubisco and the plastidial malic enzyme when bound to either metal. When Rubisco purified from five C_3 species was bound to magnesium rather than manganese, the specificity for CO_2 over O_2, ($S_{c/o}$) increased by 25% and the ratio of the maximum velocities of carboxylation / oxygenation (V_{cmax}/V_{omax}) increased by 39%. For the recombinant plastidial malic enzyme, the forward reaction (malate decarboxylation) was 30% slower and the reverse reaction (pyruvate carboxylation) was three times faster when bound to manganese rather than magnesium. Adding 6-phosphoglycerate and $NADP^+$ inhibited carboxylation and oxygenation when Rubisco was bound to magnesium and stimulated oxygenation when it was bound to manganese. Conditions that favored RuBP oxygenation stimulated Rubisco to convert as much as 15% of the total RuBP consumed into pyruvate. These results are consistent with a stromal biochemical pathway in which (1) Rubisco when associated with manganese converts a substantial amount of RuBP into pyruvate, (2) malic enzyme when associated with manganese carboxylates a substantial portion of this pyruvate into malate, and (3) chloroplasts export additional malate into the cytoplasm where it generates NADH for assimilating nitrate into amino acids. Thus, plants may regulate the activities of magnesium and manganese in leaves to balance organic carbon and organic nitrogen as atmospheric CO_2 fluctuates.

1 | INTRODUCTION

Rubisco (ribulose-1,5-bisphosphate carboxylase-oxygenase), the most prevalent protein on the planet (Bar-On and Milo 2019, Ellis 1979), catalyzes several competing chemical reactions. One reaction is the carboxylation of ribulose 1,5-bisphosphate (RuBP) to two molecules of 3-phosphoglyceric acid (3PGA) that initiates C_3 carbon fixation. Another reaction is the oxygenation of RuBP to one molecule of 3PGA and one molecule of 2-phosphoglycolate (2PG) that initiates photorespiration. In a third reaction, Rubisco converts RuBP into one molecule of pyruvate and one of 3PGA or 2-PG (Andrews and Kane 1991).

Calvin, Benson, and Bassham, as part of their seminal studies on the biochemistry of plant carbon assimilation in the 1950s, exposed the alga *Scenedesmus* to a pulse of radioactive $^{14}CO_2$. They found that

the ^{14}C label appeared in 3PGA (3-phosphoglycerate), the first stable intermediate of C_3 carbon fixation, within two seconds and in pyruvate and malate within four seconds (Benson et al. 1952). Radioactivity reached a steady level in 3PGA within two minutes but rose in pyruvate and malate for 10 minutes (Benson et al. 1952). Adding malonate to the medium inhibited malate synthesis and eliminated ^{14}C accumulation in malate but did not affect ^{14}C accumulation in 3PGA. Calvin, Benson, and Bassham concluded that the 3PGA and malate derive from two independent carboxylation reactions (Bassham et al. 1950) but never identified the carboxylation reaction that generates malate.

In recent labeling experiments, C_3 plants accumulated the stable isotope ^{13}C in pyruvate and malate only slowly after receiving a pulse of $^{13}CO_2$ (Fu et al., 2023; Ma et al., 2014; Szecowka et al., 2013; Xu et al., 2022). These studies used GC–MS to quantify pyruvate and malate after derivatizing them with methoximation, followed by tert-butyldimethylsilylation. Unfortunately, this method cannot account for a major portion of these organic acids because of peak-tailing (Arrivault et al., 2009) and matrix effects (Alseekh et al., 2021; Tarakhovskaya et al., 2023). In contrast, a study that used non-targeted ^{13}C-NMR analysis to quantify plant metabolites found that after receiving a $^{13}CO_2$ pulse under conditions that enhance photorespiration, a C_3 species accumulated more ^{13}C label in the 4th carbon of malate than in any other metabolite or any other carbon position of malate (Abadie et al. 2021).

In studies conducted over three decades ago, the binding of Rubisco to Mn^{2+} instead of Mg^{2+} inhibited RuBP carboxylation and accelerated RuBP oxygenation (Christeller, 1981; Christeller and Laing, 1979; Jordan and Ogren, 1983; Martin and Tabita, 1981; Wildner and Henkel, 1979) and slightly enhanced Rubisco pyruvate generation (Andrews and Kane. 1991). All of these studies purified Rubisco via ammonium sulfate or ethylene glycol precipitation followed by centrifugation, procedures that can adversely influence enzyme structure and activation (Iñiguez et al., 2021; Wingfield, 1998).

Rubisco from higher plants also binds 6-phosphogluconate (6PG) and $NADP^+$ near the active site where CO_2 or O_2 reacts with RuBP (Matsumura et al., 2012). Additions of moderate concentrations of 6PG or NADPH stimulate Rubisco carboxylation in the presence of Mg^{2+} (Chu and Bassham, 1973; Chu and Bassham, 1974). Binding these ligands to Rubisco increases its activation at sub-saturating concentrations of CO_2 and Mg^{2+} (Parry et al., 2008; Yokota et al., 1992). Oxidation of 6PG in chloroplasts stabilizes photosynthesis (Sharkey and Weise, 2016).

Malic enzyme catalyzes the reversible reaction (malate + $NADP^+$ ↔ pyruvate + CO_2 + NADPH) when bound to Mg^{2+} or Mn^{2+} (Chang and Tong, 2003). *Arabidopsis thaliana* and tobacco each have one isoform of malic enzyme in plastids (Müller et al., 2008; Wheeler et al., 2008). None of the T-DNA mutants defective in one of the four AtNADP-ME genes exhibited abnormal phenotypes under standard greenhouse conditions, nor did double or triple combinations of the mutations (Wheeler et al., 2005). There are no previous studies on the influence of Mn^{2+} on the behavior of the plastidial NADP-ME isoform.

The following study examines the influence of Mg^{2+} or Mn^{2+} and 6PG or NADP(H) on the behavior of Rubisco and plastidial malic enzyme using modern purification protocols that preserve the metal-binding characteristics of the proteins and developed new assays that are indifferent to the presence of Mg^{2+} or Mn^{2+}. Our results suggest that plastid carboxylation reactions generate either carbohydrates or malate in chloroplasts depending on the balance between leaf Mg^{2+} or Mn^{2+} activities.

2 | MATERIALS AND METHODS

2.1 | Plant growth conditions

We planted Arabidopsis (*Arabidopsis thaliana* cv. Col-0; ABRC Ohio State U., CS1092), rice (*Oryza sativa* cv. Kitaake; National Small Grains Collection PI 652747), wheat (*Triticum aestivum* cv. Veery 10; International Maize and Wheat Improvement Center CWI 35519), and tobacco (*Nicotiana tabacum* cv. Petite Havana; North Carolina State U. Tobacco Germplasm Collection PI 552516) seeds into 5 × 5 cm containers containing Sunshine Mix 4 (Sungro, Agawam). The plants grew in a controlled environmental chamber for 21 d under 450 ppm CO_2, 50%/70% relative humidity (light/dark), an air temperature of 22°/18°C (light/dark), and 16 h of 600 µmol m^{-2} s^{-1} PPFD at canopy height. For spinach Rubisco, we purchased *Spinacia oleracea*, Taylor Farms tender spinach leaves, from a local Costco Wholesale store.

2.2 | Rubisco extraction and purification

We collected about 40 g of leaves of each species and froze them in liquid N_2. Manual grinding with a mortar and pestle pulverized the plant material to a fine powder. We extracted the fine powder in 100 mL of a buffer (50 mM Tris–HCl pH 7.4, 20 mM $MgCl_2$, 20 mM $NaHCO_3$, 0.1 mM Na_2EDTA, 10% glycerol, 50 mM mercaptoethanol, and 1 mM PMSF), filtered the extract through four layers of Miracloth, centrifuged it at 12 100 *g*, 4°C for 15 min to clarify it, and passed the supernatant through a 0.22 µm syringe filter before loading it onto an NGC™ FPLC system (BioRad).

We purified Rubisco using an ENrich™ SEC (Size Exclusion Column) 650 10 × 300 Column (BioRad) followed by a HiScale 16/20 6 mL SOURCE 30Q column (GE Healthcare Life Sciences). All buffers included 2 mM dithiothreitol to prevent intermolecular disulfide bond formation. Pre-equilibration of the size exclusion column involved eluting five column volumes (CV) of 85% buffer A (50 mM Tris–HCl, 1 mM EDTA, 0.1 mM PMSF, pH 7.4) and 15% buffer B (50 mM Tris–HCl, 1 M NaCl 1 mM EDTA, 0.1 mM PMSF, pH 7.4). We loaded the protein sample onto the column and eluted it with 2 CV of 15% buffer B. UV absorption at 280 nm confirmed the protein peak. We (a) concentrated the protein solution to around 1 mM, (b) exchanged the buffer into buffer A, (c) filtered the sample, (d) loaded it onto a SOURCE 30Q column pre-equilibrated with 5 CV of buffer A, (e) eluted the protein with 50% buffer B with a linear gradient over

10 CV, (f) pooled the protein peak at 280 nm, (g) exchanged the buffer into buffer A with the addition of 20% glycerol and (h) stored the protein solution at −80°C. We checked the purity of the protein on SDS-PAGE gels, Western Blots, and an Evolution 201 UV/Vis spectrometer coupled with an Evolution 1-cell Peltier temperature control system (Thermo Fisher Scientific).

2.3 | Rubisco carboxylation colorimetric reaction

A standard approach for estimating the V_{cmax} (maximum carboxylation activity) and turnover rate of Rubisco in vitro is a colorimetric analysis of 3PGA (3-phosphoglycerate) via a coupled enzyme assay. One such coupled enzyme system is (Lilley and Walker, 1974; Sharkey et al., 1991):

$$\xrightarrow{\text{Rubisco}} 3\text{PGA} \xrightarrow{\text{3PGA kinase}} \text{bis-PGA} \xrightarrow{\text{GAPDH+NADH}} \text{Ga-3-P} + \text{NAD} \xrightarrow{\text{TIM}} \text{DHAP}$$
$$\xrightarrow{\text{GlyPDH+NADH}} \text{Gly-3-P} + \text{NAD}$$

where (a) 3PGA kinase phosphorylates 3PGA to produce bis-PGA that (b) GAPDH (glyceraldehyde-3-P dehydrogenase) and NADH reduce to the aldehyde Ga-3-P, (c) TIM (triose-phosphate isomerase) converts Ga-3-P to di-hydroxyacetone phosphate (DHAP) that (d) GlyPDH (glycerol-P dehydrogenase) and NADH reduce to Gly-3-P. Estimates of Rubisco activity are based on the changes in NADH concentration as measured on a UV/vis spectrophotometer (Thermo Fisher Scientific) by their absorbance at 340 nm. Unfortunately, this method fails to consider oxygenation reaction rates in calculating the carboxylation rates of Rubisco. Moreover, most of the enzymes used in this assay require the presence of Mg^{2+} and may not function in the presence of Mn^{2+} (Beleznai et al., 1988; Greinert et al., 2020; Varga et al., 2012).

We developed a different colorimetric assay for Rubisco carboxylation that is accurate in the presence of Mg^{2+} or Mn^{2+}:

$$\xrightarrow{\text{Rubisco}} \text{3-PGA} \xrightarrow{\text{iPGM}} \text{2-PGA} \xrightarrow{\text{Enolase}} \text{PEP} \underset{\text{ADP}}{\overset{\text{PK}}{\rightleftarrows}} \underset{\text{ATP}}{\text{pyruvate}} \xrightarrow[\text{phosphate} + \text{O}_2]{\text{pyruvate oxidase}} \underset{\text{acetyl phosphate} + \text{CO}_2}{\text{H}_2\text{O}_2} \xrightarrow{\text{HRP + Amplex Red}} \text{resorufin}$$

To estimate v_c and V_{cmax}, we assessed Rubisco production of 3PGA from RuBP in the presence of high levels of CO_2, iPGM (cofactor-Independent PhosphoGlycerate Mutase) conversion of 3PGA to 2PGA (Raverdy et al., 2007; Zhang et al., 2004), followed by a commercial assay kit (2-phosphoglycerate Assay kit, Abcam ab174097) that converts 2PGA into PEP, then to pyruvate, H_2O_2, and resorufin. Absorption at 570 nm monitored resorufin production. This assay can detect 2PGA levels below 20 pmol and works in the presence of either metal cofactor (Figure S1).

In more detail, we activated Rubisco before the assays as follows. We added an assay buffer containing 20 mM Tris–HCl, 1 mM EDTA, 100 mM Triethanolamine at pH 7.8 to one 5 mL tube; added 1 or 2 µL of Rubisco (0.5–1 µM), 10 µL of 250 mM $NaHCO_3$, 0.5 µL carbonic anhydrase (~2.5 units), 5 µL of iPGM (10 µM), 4 µL of $MgCl_2$ (final concentration 20 mM) or $MnCl_2$ (5 mM); mixed everything thoroughly and allowed the mixture to sit for 5 minutes. The final assay volume in the tube was 1750 µL. We started the reaction by adding 45 µL of 10 mM RuBP to the tube, split the mixture into five tubes, and stopped the reaction after 1, 2, 3, 4, or 5 mins by adding 0.5 N HCl to each tube. We added KOH to each reaction tube to adjust the pH to about pH 7.8 and added to the tubes equal amounts of freshly mixed 2PGA colorimetric cocktail that we prepared from a 2-phosphoglycerate assay kit (ab174097, Abcam), mixed all tubes well, and moved the tubes to an opaque box. We measured OD_{570nm} after 40 min for each of the tubes and calculated the 2PGA concentration in each reaction tube based on a calibration curve determined by adding specified quantities of a 1 mM 2PGA standard solution that the assay kit provided.

The carboxylation turnover rate $v_c = ½$ (resorufin production rate − v_o), where we estimated v_o, the O_2 depletion rate, as detailed in the section below on "Rubisco oxygenation".

We estimated V_{cmax} from the Michaelis–Menten equation:

$$v_c = \frac{[CO_2] \cdot V_{cmax}}{[CO_2] + K_c(1 + [O_2]/K_o)}$$

and the relative specificity $S_{c/o}$ from:

$$S_{c/o} = \frac{V_{cmax} K_o}{V_{omax} K_c}.$$

We conducted separate calibration runs in the presence of the buffer and Mg^{2+} or Mn^{2+} in the same concentrations used in the Rubisco reactions (Figure S1) and calculated the ratio between the slopes of the runs using only the 2PGA buffer and the slopes of the runs containing Rubisco. Linear regressions for each combination of plant and metal ion, which included a constant term for each run, expressed the change in 2PGA as a function of time.

2.4 | IPGM expression and purification

We transformed a 6xHis-tagged *C. elegans* nematode iPGM plasmid into BL21(DE3) competent cells and incubated them at 37°C overnight. We selected one colony for culturing at 37°C overnight in 50 mL LB media (peptone 10 g, yeast extract 5 g, NaCl 10 g l^{-1}) and 50 µL 100 g ml^{-1} kanamycin stock solution. We added 10 mL of the small culture to 1 L of the same media and grew it until $OD_{600} = 0.7$. We added isopropyl β-D-1-thiogalactopyranoside (IPTG) to the culture flask to bring it to a final concentration of 0.2 mM and reduced the temperature and stirring speed to 30°C and 0.14 *g*, respectively. We grew the culture for 24 h, centrifuged it for 20 min at 4700 *g*, and suspended the pellet in 30 mL buffer A (20 mM Tris–HCl, 2 mM DTT, pH 6.8). We stored the cell suspension at −80°C before purification.

We thawed 30 mL of the cell suspension, lysed the cells by adding 30 mg of lysozyme and 30 µg of DNAse, and passed the cells twice through a French press. We centrifuged the solution at

12 100 *g* for 60 min, concentrated the supernatant using Amicon Ultra Centrifuge Filters (EMD Millipore), and filtered the resulting solution using a 0.22 μm filter before loading it onto a column.

We pre-equilibrated a Bio-Scale Mini Profinity IMAC cartridge with five column volumes (CV) of buffer A (50 mM Tris–HCl, 25 mM imidazole, 1 mM EDTA, 0.1 mM PMSF, pH 7.4), loaded the protein sample onto the column, washed the column with 5 CV of buffer A, and eluted the protein with a linear gradient over 10 CV of buffer B (50 mM Tris–HCl, 500 mM imidazole, 1 mM EDTA, 0.1 mM PMSF, pH 7.4), and confirmed the protein peak by monitoring UV absorption at 280 nm. We stored the fractions at −80°C.

2.5 | Rubisco oxygenation

Most studies that directly measure Rubisco oxygenation use a polarographic (Clark style) O_2 electrode to monitor oxygen depletion (Badger and Andrews, 1974; Carmo-Silva et al., 2010; Makino et al., 1988; Martin and Tabita, 1981; Wildner and Henkel, 1979). This instrument has several drawbacks. The electrode itself consumes oxygen (Clark et al., 1953; Severinghaus and Astrup, 1986; Wolfbeis, 2015), potentially leading to inaccurate results when used over time. The membrane separating the electrode from the environment causes a delay of at least 3 to 10 s in responding to changes in O_2 concentration (Pouvreau et al., 2008). The accuracy of the electrode declines and its response time increases with higher temperatures (Miniaev et al., 2013) and it is sensitive to light (Hitchman, 1978). Another way to assess oxygenation directly is MIMS (Membrane Inlet Mass Spectrometry). This method can simultaneously measure carboxylation and oxygenation and avoids some difficulties with Clark electrodes, but has other drawbacks. It is a very complex method, requires time-consuming measurements, involves a closed system that needs correction for membrane isotopic discrimination, and has low reproducibility: several recent studies found that MIMS-derived catalytic rates for Rubisco carboxylation, oxygenation, and CO_2/O_2 specificity were inconsistent with values derived from radiolabel measurements for reasons that are still undetermined (Boyd et al., 2019; Iñiguez et al., 2021; Sharwood et al., 2016).

To avoid these problems, we used a newly available needle-type oxygen micro-optode OXF50-OI (PyroScience GmbH). In this instrument, a polymer optical fiber transmits a fluorescence excitation wavelength to the tip of the sensor while it concurrently transmits the fluorescence response of an oxygen-sensitive dye in a polymer matrix at the tip. The oxygen concentration determines the quenching of the excitation light. The micro-optode has a 50 μm tip diameter, facilitating a micro-scale setup such as in a micro-cuvette or plate. The most important advantages of this type of sensor are that it does not consume O_2, has no stirring sensitivity, and is resistant to most corrosive environments (Clark et al., 1953; Severinghaus and Astrup, 1986; Wolfbeis 2015). The micro-optode also works in both gas (% O_2) and liquid phases (DO), which makes it possible to measure O_2 exchanges accurately at up to 250% air O_2 saturation in intact plant leaves, bioreactors, cell cultivations, microtiter plates, and many liquids (Bentzon-Tilia et al., 2015; Bittig et al., 2018; Fischer et al., 2014; Flitsch et al., 2016; Helm et al., 2018; Ortner et al., 2015).

A needle-type micro-optode OXF50-OI (PyroScience GmbH) on a FireSting O_2 optical oxygen and temperature meter (FSO2-4) monitored changes in O_2 concentration in a spectrophotometer 3.5 mL quartz cuvette (Millipore Sigma) during our Rubisco oxygenation experiments. We conducted these experiments under three sets of conditions at 25°C: (a) ambient air (79% N_2, 20.96% O_2, and 0.04% CO_2), (b) elevated CO_2 content (78.96% N_2, 20.96% O_2, and 0.08% CO_2), and (c) reduced O_2 content (89% N_2, 10.96% O_2, and 0.04% CO_2). Precision mass flow controllers (Apex Vacuum) calibrated against soap bubble flowmeters mixed pure N_2, O_2, and CO_2 to the desired concentrations. A non-dispersive Infrared Gas Analyser (Li-cor) checked the CO_2 concentration. We conducted a two-point calibration of the oxygen optode in both air and air-saturated water. The final assay volume in each tube was 3000 μL.

Before the oxygenation assay, we activated Rubisco as follows: we added assay buffer (20 mM Tris–HCl, 1 mM EDTA, 10 mM $NaHCO_3$, 100 mM triethanolamine, pH 7.8) to a covered, temperature-controlled, 4 mL quartz cuvette; added 10 μL of Rubisco (0.5–1 μM), 50 μL of iPGM (10 μM), 5 μL carbonic anhydrase (~25 units), and 40 μL of $MgCl_2$ (final concentration 20 mM) or $MnCl_2$ (5 mM) and mixed the contents of the cuvette thoroughly. We allowed the mixture to sit for 5 minutes before inserting the oxygen sensor and sparging it for 1 minute with the gas mixture corresponding to the experiment's conditions. After about 30 s, once the oxygen sensor reading stabilized, we started the reaction by adding 100 μL of 10 mM RuBP (pre-equilibrated with the same gas mixture) and began collecting data. We did not observe any apparent protein deactivation and degradation during more than 300 s. Therefore, we estimated the oxygenation turnover rate v_o from the linear trend in oxygen consumption for at least 200 s divided by Rubisco content.

Michaelis–Menten kinetics predicts the oxygenation turnover rate v_o to be:

$$v_o = \frac{[O_2] \cdot V_{omax}}{[O_2] + K_o(1 + [CO_2]/K_c)}$$

where V_{omax}, K_o, and K_c depend on species and the associated metal, Mn^{2+} or Mg^{2+}, but are independent of $[O_2]$ and $[CO_2]$. Values of v_o under multiple sets of conditions for $[O_2]$ and $[CO_2]$, therefore provided estimates of the three parameters V_{omax}, K_o, and K_c (Table S1). For the reduced O_2 experiments, we performed blank runs with RuBP and all other components but without Rubisco. We calculated O_2 consumption rates before and after adding RuBP for both the blank and actual runs and determined the O_2 consumption rate as

$$O_2\ consumption = R_{Rubisco,RuBP} - R_{Rubisco} - (R_{RuBP} - R_{Neither})$$

where R denotes the rate of change in oxygen levels in the presence or absence of Rubisco and RuBP.

2.6 | Rubisco pyruvate generation

Quantifying pyruvate via gas chromatography/mass spectroscopy is error-prone because of peak tailing (Arrivault et al., 2009) and matrix effects (Alseekh et al., 2021; Tarakhovskaya et al., 2023). Therefore, GC/MS cannot account for most of the pyruvate in *Arabidopsis thaliana* leaves (Alseekh et al., 2021). Metabolomic studies of plants often quantify pyruvate through enzymatic reactions that oxidize NAD(P)H (Arrivault et al., 2009). Initially, we assessed Rubisco generation of pyruvate from RuBP via an assay catalyzed by lactate dehydrogenase in which pyruvate + NADH → lactate + NAD^+ (Andrews and Kane, 1991; Hatzfeld et al., 1990). We used a buffer containing 130 mM Hepps-NaOH, pH 8.3, 18 mM $MgCl_2$, 50 pM NADH, and 1 mM RuBP and sparged it with N_2 to make it CO_2- and O_2-free. After stopping the sparging, we added 0.05–20 mM HCO_3^-, 100 pg ml^{-1} bovine erythrocyte carbonic anhydrase, and 3 units ml^{-1} rabbit muscle lactate dehydrogenase, and started the reaction by adding tobacco Rubisco that we preactivated in the presence of 19 mM $MgCl_2$ and 10 mM $NaHCO_3^-$. We monitored the extent of NADH oxidation at 25°C from the change in absorption at 340 nm.

Subsequently, we shifted to a commercial pyruvate assay kit based on pyruvate oxidase generation of hydrogen peroxide from pyruvate (BioAssay Systems, 2022). We mixed a solution containing 12.5 mM $NaHCO_3$, either 15 mM $MgCl_2$ or 3.75 mM $MnCl_2$, 5 units ml^{-1} carbonic anhydrase, and 8% purified Rubisco solution with an assay buffer (20 mM Tris–HCl, 1 mM EDTA, 100 mM Triethanolamine, pH 7.8) and allowed it to sit for 5 minutes to activate Rubisco. For ambient experiments, we subsequently purged it for 5 minutes with ambient air. For experiments on the influence of 6PG and/or $NADP^+$, 400 μM 6PG and/or $NADP^+$ was added, respectively. We started all experiments by adding 8 μM RuBP, removed samples immediately and after 3, 6, 9, and 12 minutes, and stopped the experiment by heating to 80°C. We centrifuged the samples for 3 minutes in a tabletop microcentrifuge at 21 100 *g*, extracted the liquid, and used a commercial kit to assess pyruvate via pyruvate oxidase generation of hydrogen peroxide that reacted with nonfluorescent Amplex Red at a 1:1 stoichiometry and formed the fluorescent product resorufin. We measured resorufin with a Horiba Fluorolog at $\lambda_{em/ex}$ = 585/530 nm (Zhu et al. 2010). This assay indicated that Rubisco pyruvate generation was more than 10 times faster than in our earlier measurements using lactate dehydrogenase: Rubisco converted more than 6% of the RuBP into pyruvate (Zhu et al. 2010).

2.7 | Recombinant plastidial malic enzyme expression, purification, and kinetics

We transformed the *E. coli* BL21 (DE3) strain c41, which contains a mutation in the lacUV5 promoter that makes it a weaker promoter, with a plasmid containing the 6xHis-tagged sequence for At-NADP-ME-4 from *Arabidopsis thaliana*. The *plastidial* transit peptide (pTP) was removed from the plasmid sequence. The transformed colonies were grown in LB agar containing 100 μg ml^{-1} ampicillin overnight. One colony was selected and grown in 50 mL of LB media (peptone 10 g, yeast extract 5 g, NaCl 10 g l^{-1}) overnight at 37°C. We added 5 mL of the small culture to 500 mL of the same media and grew it at 30°C until OD_{600} = 0.6 before inducing the plasmid with 1% lactose overnight (~16 h) at a temperature of 18°C. We harvested the cells by centrifuging at 5000 *g* for 1 hour at 4°C and resuspended the pellet in 20 mL of 20 mM Tris–HCl, 0.25 M NaCl, 0.01% (v/v) Triton X-100 and 1 mM PMSF, pH 7.5. We sonicated the resuspension for three pulses of 15 seconds by an ultrasonic cell disruptor and then centrifuged it for 10 minutes at 14 000 *g* at 4°C to separate the supernatant from the pellet. We loaded the uninduced control culture, induced culture, supernatant, and pellet onto a SDS-PAGE and measured NADP-ME activity on the crude extracts.

We pre-equilibrated a EconoFit Profinity IMAC cartridge (BioRad) with five column volumes (CV) of buffer A (20 mM Tris–HCl, 0.25 M NaCl, 0.01% (v/v) Triton X-100, 10 mM imidazole, 10% glycerol, 1 mM DTT, pH 8), loaded the protein sample onto the column, washed the column with 5 CV of buffer A, and eluted the protein with a linear gradient over 10 CV of buffer B (20 mM Tris–HCl, 0.25 M NaCl, 0.01% (v/v) Triton X-100, 500 mM imidazole, 10% glycerol, 1 mM DTT, pH 7.5). All elution fractions were saved and loaded onto a SDS-PAGE. The protein identity was confirmed by western blot and activity assays. We flash froze and stored the fractions with protein of interest at −80°C.

For malic enzyme malate oxidative decarboxylation reactions, we added a buffer (50 mM MOPS pH 7.3, 0.25 M NaCl, 0.01% (v/v) Triton X-100 and 1 mM DTT) to a quartz cuvette along with purified malic enzyme (3.5–5.0 μg ml^{-1} as measured by a Bradford assay). To this mixture, we added 10 mM $MgCl_2$ or 1.7 mM $MnCl_2$ and 500 μM $NADP^+$ and started the reaction by adding 10 mM malate as a final concentration.

For pyruvate reductive carboxylation reactions, we used the same buffer and protein. To this mixture, we added 10 mM $MgCl_2$ or 1.7 mM $MnCl_2$, 30 mM $NaHCO_3$, and 100 μM NADPH and started the reaction by adding 50 mM pyruvate (final concentration).

In both cases, we monitored the reaction on a UV/Vis spectrophotometer at 1-minute intervals (Figure S3), averaged the absorbances for wavelengths between 330 and 345 nm to estimate the quantity of NADPH produced or consumed, and estimated the reaction rate via a linear regression over a 10-minute period.

2.8 | Statistics

In general, we used R for Windows version v.4.0.5 and will provide the R code upon request. For the two-way ANOVA on the influence of atmospheric CO_2 level and N source on the manganese to magnesium ratio in wheat leaves (Table S8) we used the SAS PROC MIXED version 9.4 and will provide the code upon request.

From the measured rates of Rubisco reactions, kinetic parameters were calculated using a Bayesian method. Briefly, random sets of kinetic parameters were generated from a lognormal prior distribution, based on the approximate range in which kinetic parameters for C_3

plants have been calculated, and the relative likelihood of observing the values in our experiments was computed for each set of kinetic parameters. The result of each experiment was assumed to be normally distributed with a fixed variance, combining the regression standard error in the measurements with the variance between the results of similar experiments. These likelihoods were used as weights to approximate a posterior distribution on the kinetic parameters from which we calculated posterior means and standard deviations of each parameter.

To determine the overall effects of Mg^{2+} and Mn^{2+} across plant species, we aggregated each kinetic parameter, adjusted by their respective standard errors, and used it as input to a two-way ANOVA, with metal ion and plant species as variables. (Table S1).

For calculations of the effect of $NADP^{+}$, NADPH, and 6PG on Rubisco kinetics, we performed parallel experiments in order to account for daily variation in the measured reaction rates. For each combination of metal and ligand, we conducted 5–11 replications of the oxygenation measurements and 5–8 replications of the total reaction measurement. We compared these replications with runs on the same day in the absence of any of these ligands and recorded the differences in rates (Figure 3). ANOVA and a Tukey test compared these values among different ligands (Tables S3 and S4).

For Rubisco pyruvate production, we performed 4–6 replications with each combination of metal, CO_2 level, and presence or absence of 6PG and presented the rates of pyruvate production as a percentage of Rubisco activity estimated from previous results (Figure 4). ANOVA and a Tukey test compared these values between each combination of factors (Tables S5 and S6).

For malic enzyme activity, we performed 14 replications each of the forward reaction (malate decarboxylation) and reverse reaction (pyruvate carboxylation) in the presence of each metal and recorded the rate for each experiment. A Tukey test provided a comparison between the rates of each reaction in the presence of Mg^{2+} and Mn^{2+} (Table S7).

3 | RESULTS

3.1 | Rubisco Kinetics

The maximum velocity of carboxylation V_{cmax} was 27% faster when Rubisco was bound to Mg^{2+} rather than Mn^{2+} (Figure 1A). In contrast, the influence of Mg^{2+}vs. Mn^{2+} on the maximum velocity of oxygenation V_{omax} varied with species (Figure 1B). K_c (the Michaelis constants of Rubisco for CO_2) was 23% greater when the enzyme was bound to

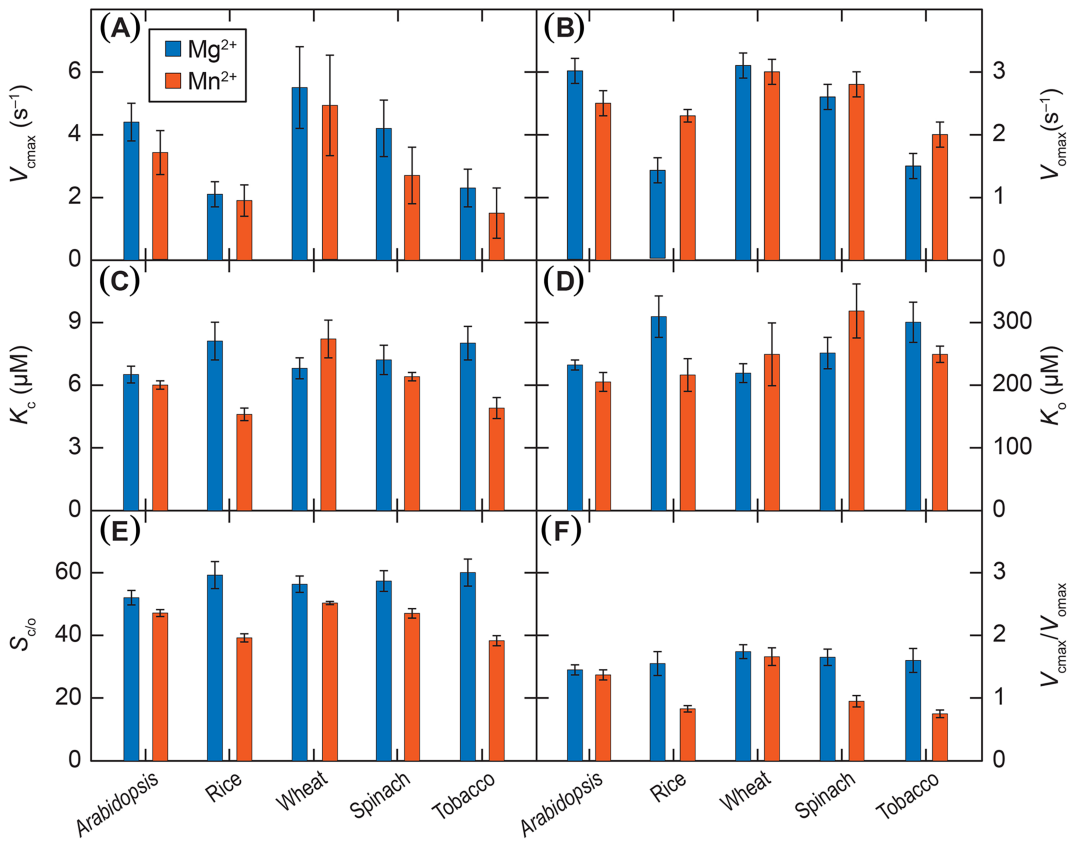

FIGURE 1 Kinetic parameters of Rubisco purified from five C_3 species (Arabidopsis, rice, wheat, spinach, and tobacco), measured in vitro at 25°C when activated Rubisco was associated with Mg^{2+} or Mn^{2+}. (A) V_{cmax} is the maximum velocity of carboxylation, (B) V_{omax} is the maximum velocity of oxygenation, (C) K_c is the Michaelis constant of Rubisco for CO_2, (D) K_o is the Michaelis constant of Rubisco for O_2, (E) $S_{c/o}$ is the specificity of Rubisco for CO_2 over O_2, and (F) V_{cmax}/V_{omax} is the ratio of the maximum velocities. Depicted here are mean ± credible interval, $n = 4$ to 20. See Table S2 for the statistical analysis of an ANOVA on the influence the two metals and five species on these parameters.

Mg^{2+} rather than Mn^{2+} (Figure 1C), and K_o (the Michaelis constants of Rubisco for O_2) varied with species (Figure 1D). $S_{c/o}$ (Rubisco specificity for CO_2 over O_2) was 25% greater when the enzyme was bound to Mg^2 rather than Mn^{2+}, and V_{cmax}/V_{omax} was 39% greater when the enzyme was bound to Mg^2 rather than Mn^{2+}. (Figures 1E & F).

Adding 6PG + $NADP^+$ to tobacco Rubisco inhibited carboxylation and oxygenation when the enzyme was bound to Mg^{2+} and stimulated oxygenation when it was bound to Mn^{2+} (Figure 2). Adding just 6PG to tobacco Rubisco stimulated carboxylation and oxygenation when the enzyme was bound to Mn^{2+} (Figure 2). Adding $NADP^+$ alone stimulated carboxylation when Rubisco was bound to Mg^{2+} and stimulated oxygenation when the enzyme was bound to Mn^{2+} (Figure 2). Adding NADPH alone did not affect Rubisco carboxylation or oxygenation, irrespective of the metal present (Figure 2). The ratio of carboxylation to oxygenation did not change significantly with the metal nor with the addition of 6PG, $NADP^+$, or NADPH (Figure 2).

3.2 | Rubisco Generation of Pyruvate from RuBP

When we assessed pyruvate via pyruvate oxidase generation of hydrogen peroxide and saw that Rubisco generation of pyruvate was a greater percentage of total RuBP consumed (a) at ambient CO_2 instead of elevated CO_2, (b) with tobacco Rubisco associated with Mn^{2+} instead of Mg^{2+}, and (c) in the presence of moderate amounts of 6PG instead of the absence of 6PG (Figure 3; Tables S4 & S5, $p < 0.001$). Therefore, conditions that favor RuBP oxygenation over carboxylation stimulated Rubisco conversion of RuBP into pyruvate. Adding NADPH interferred with the pyruvate oxidase assay (data not shown). When we assessed pyruvate via lactate dehydrogenase, the influence ambient vs. elevated CO_2, Mn^{2+} vs. Mg^{2+}, and presence vs. absence of 6PG on pyruvate generation were not consistent (Figure S2).

3.3 | Malate Generation

We characterized both malate oxidative decarboxylation (forward reaction) and pyruvate reductive carboxylation (reverse reaction) when recombinant plastidial NADP-malic enzyme (Arab-ME4) was bound to Mg^{2+} or Mn^{2+} at pH 7.3. The forward reaction was faster when Arab-ME4 was bound to Mg^{2+} than Mn^{2+}, whereas the reverse reaction was faster with Mn^{2+} than Mg^{2+} (Figure 4). In the presence of either Mg^{2+} or Mn^{2+}, the forward reaction was faster than the reverse reaction (Figure 4).

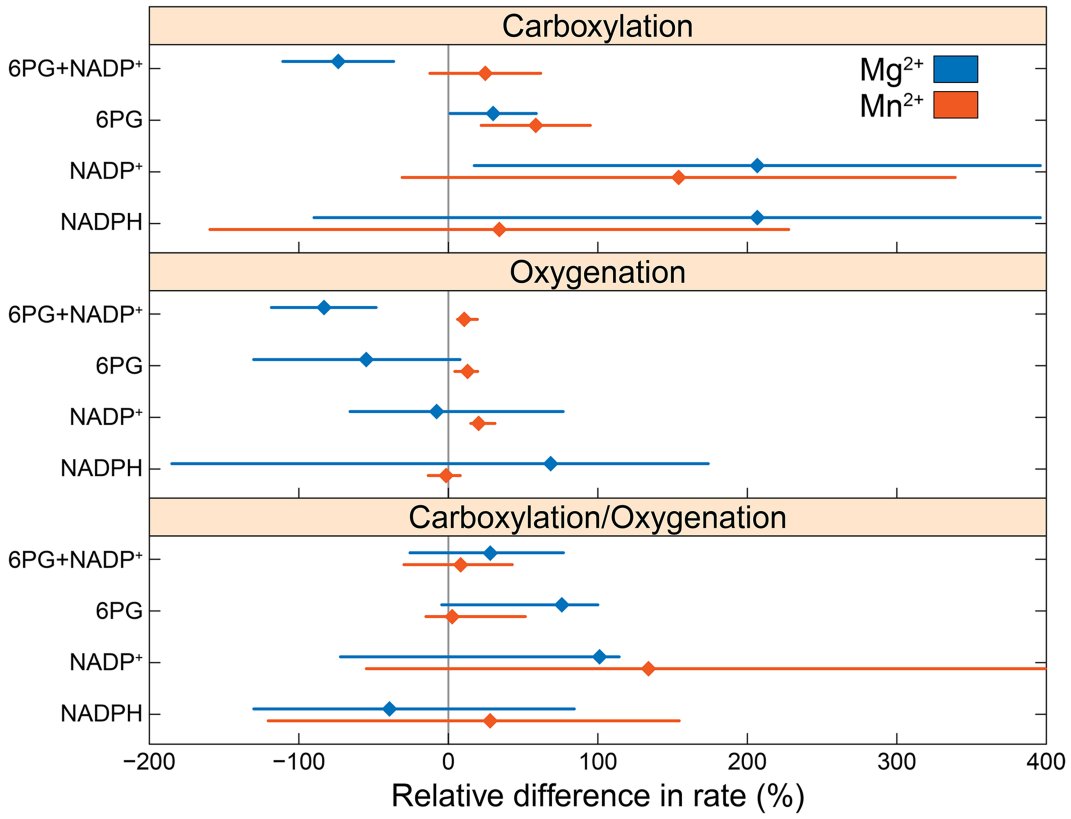

FIGURE 2 Influence of adding ligands on rates of RuBP carboxylation, oxygenation, or ratio of carboxylation over oxygenation. Values for tobacco Rubisco associated with Mg^{2+} or Mn^{2+} and aerated with 400 ppm CO_2 and 21% O_2. Change in relative rates ± confidence intervals ($n = 5$ to 11) after adding 6PG + $NADP^+$, 6PG, NADPH, or $NADP^+$. See Tables S3 and S4 for the statistical analysis of carboxylation and oxygenation.

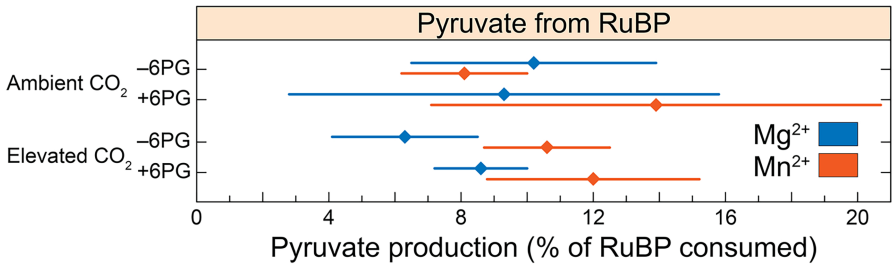

FIGURE 3 Pyruvate generation from RuBP (mean ± SE, $n = 6–11$) when tobacco Rubisco was associated with Mg^{2+} or Mn^{2+}, 21% O_2, 0 or 1 mM 6PG, and aerated with 400 ppm CO_2 or saturated with CO_2. An EnzyChrom™ Pyruvate Assay Kit that contains pyruvate oxidase and Amplex Red assessed pyruvate (BioAssay Systems 2022). We monitored fluorescence at 585 nm under 530 nm excitation. See Tables S5 and S6 for the statistical analysis of these data.

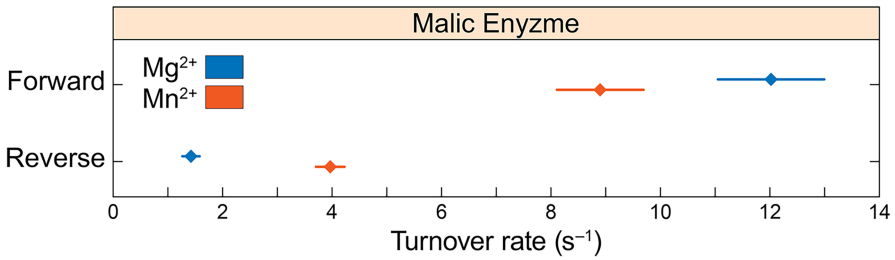

FIGURE 4 Turnover rates (mean ± SE, $n = 14$) of recombinant Arab-ME4. We measured these rates in the malate oxidative decarboxylation direction (Forward) or in the pyruvate reductive carboxylation direction (Reverse) when the enzyme is associated with Mg^{2+} or Mn^{2+}. See Table S7 for the statistical analysis of these data.

4 | DISCUSSION

4.1 | Influence of metals and other ligands on Rubisco carboxylation and oxygenation

The values for the kinetic parameters of Rubisco when bound to Mg^{2+} that we obtained using our new methods are similar to those reported previously using methods that required the presence of Mg^{2+} (Table S1). Only a handful of studies conducted more than four decades ago have evaluated Rubisco kinetics when the enzyme is bound to Mn^{2+} (Christeller, 1981; Christeller and Laing, 1979; Jordan and Ogren, 1983; Martin and Tabita, 1981; Wildner and Henkel, 1979). These studies purified Rubisco using ammonium sulfate precipitation followed by centrifugation, a purification method that can adversely influence enzyme structure and activation (Iñiguez et al., 2021; Wingfield, 1998). Perhaps as a result, these studies reported kinetic parameters for Rubisco bound to Mn^{2+} that vary more than ten-fold (Christeller, 1981; Christeller and Laing, 1979; Jordan and Ogren, 1983; Martin and Tabita, 1981; Wildner and Henkel, 1979). Carboxylation and oxygenation of RuBP when Rubisco is bound to Mn^{2+} could involve mechanisms different from those when it is bound to Mg^{2+} (Bathellier et al., 2020).

Here, we purified Rubisco using gel filtration and ion exchange columns in a modern, fast protein liquid chromatographic system (NGC™, BioRad). We first subjected the enzyme to extensive buffer exchange by ultrafiltration during the assays of Rubisco bound to Mn^{2+} to remove any associated Mg^{2+} and then activated Rubisco by exposure to Mn^{2+}. In our experiments, Rubisco had similar V_{omax}, K_c, and K_o when bound to Mg^{2+} and Mn^{2+} (Figure 1), attesting to the efficacy of our Rubisco purification and activation protocols.

The addition of 6PG may stimulate Rubisco carboxylation of RuBP if the enzyme is activated and the concentration of 6PG is below 1 mM, and may inhibit Rubisco carboxylation if the enzyme is not activated or when the concentration of 6PG exceeds 1 mM (Chu and Bassham, 1973; Chu and Bassham, 1974). Our experiments preactivated Rubisco, so the stimulation of Rubisco carboxylation by adding 0.4 mM 6PG concentration (Figure 2) is consistent with prior experiments.

4.2 | Influence of metals and other ligands on Rubisco generation of pyruvate

Methods for analyzing pyruvate can be problematic. Peak tailing (Arrivault et al., 2009) and matrix effects (Alseekh et al., 2021; Tarakhovskaya et al., 2023) interfere with Gas Chromatographic/Mass Spectroscopic approaches. Therefore as an alternative, metabolomic studies of plants often quantify pyruvate through enzymatic reactions that oxidize NAD(P)H (Arrivault et al., 2009). We initially assessed Rubisco generation of pyruvate from RuBP via an assay catalyzed by lactate dehydrogenase in which pyruvate + NADH → lactate + NAD^+ (Andrews and Kane, 1991; Hatzfeld et al., 1990). This assay indicated that Rubisco generation of pyruvate was less than 0.5% of the RuBP consumed (Figure S2). Other studies that used this assay obtained similar results (Andrews and Kane, 1991; Treves et al., 2022).

We suspected that these low rates of pyruvate generation derived from the inhibition of Rubisco by lactate, NADH, or lactate dehydrogenase (Cannon et al., 2021) and therefore shifted to a commercial pyruvate assay (BioAssay Systems, 2022) based on pyruvate oxidase generation of hydrogen peroxide that reacts with nonfluorescent Amplex Red at a 1:1 stoichiometry to form the fluorescent product resorufin (Zhu et al., 2010). We measured resorufin with a Horiba Fluorolog at $\lambda_{em/ex} = 585/530$ nm. This assay indicated that Rubisco converted more than 6% of the RuBP into pyruvate (Figure 3), more than 10 times faster than in our earlier measurements using lactate dehydrogenase.

Andrews and Kane hypothesized that Rubisco generated pyruvate by beta elimination from the fragment of RuBP formed from the top three carbons followed by cleavage (Andrews and Kane, 1991). We found that conditions favoring RuBP oxygenation stimulated Rubisco pyruvate generation (Figure 3), indicating that pyruvate derives from the bottom three carbons of RuBP. Determining which of these two possibilities is prevalent will require further experimentation.

4.3 | Malate generation in chloroplasts

Our results suggest a stromal biochemical pathway in which (a) Rubisco generates pyruvate during RuBP oxygenation (Andrews and Kane, 1991); (b) phosphogluconate dehydrogenase decarboxylates 6PG to produce Ru5P, CO_2, and NADPH (Lew et al., 2014) and (c) malic enzyme carboxylates the pyruvate generated by the first reaction using the CO_2 and NADPH generated by the second reaction to produce malate (Figures 2–4; Brown and Cook, 1981; Chang and Tong 2003, Müller et al., 2008; Wheeler et al., 2008).

The proposed pathway has remained unrecognized because current mass spectrometric and enzymatic methods (Alseekh et al., 2021; Andrews and Kane, 1991; Arrivault et al., 2009; Hatzfeld et al., 1990) grossly underestimate plastid pyruvate generation (Figures S2, 3). Moreover, the proposed pathway becomes prominent only when the plastid enzymes Rubisco and malic enzyme are bound to Mn^{2+}, but nearly all experiments involving Rubisco and malic enzyme promote net CO_2 assimilation by removing Mn^{2+} from these enzymes and replacing it with Mg^{2+} (Bloom and Kameritsch 2017; Bloom and Lancaster 2018; Shi and Bloom 2021).

Excluding Mn^{2+} from plastid reactions seems incongruous with the evolution of oxygenic photosynthesis and the Great Oxidation Event that began 2.3 to 2.5 billion years ago. These developments co-occurred with the increase in soluble Mn^{2+} near Earth's surface (Fischer et al., 2016; Lingappa et al., 2019) and depended on the proliferation of photosynthetic organisms having particular attributes. These attributes include (a) an Mn^{2+} complex in photosystem II that splits water and releases O_2 (Fischer et al., 2016; Lingappa et al., 2019), (b) Mn^{2+}-containing compounds that provide cellular protection against oxidative stress (Fischer et al., 2016; Lingappa et al., 2019), (c) a Form I Rubisco that has more than one hundred times greater affinity for Mn^{2+} than Mg^{2+} (Bloom and Kameritsch, 2017), and (d) photorespiratory reactions that accelerate when the enzymes involved are bound to Mn^{2+} instead of Mg^{2+} (Christeller, 1981; Christeller and Laing, 1979; Hagemann et al., 2016; Jordan and Ogren, 1983; Martin and Tabita, 1981; Segura-Broncano et al., 2023; Wildner and Henkel, 1979).

Mg^{2+} activity in tobacco chloroplasts is about 8 mM, whereas Mn^{2+} activity is about 80 μM (Bloom and Kameritsch, 2017). A tenfold increase in Mg^{2+} activity of the medium increased chloroplast Mg^{2+} activity by tenfold. In contrast, a tenfold increase in Mn^{2+} activity of the medium increased chloroplast Mn^{2+} activity by only three-fold (Bloom and Kameritsch 2017). This result implies that the chloroplast membrane has a more significant role in regulating the activity of Mn^{2+} than Mg^{2+} in chloroplasts. Isothermal titration calorimetry estimated that Rubisco purified from tobacco had a higher dissociation constant (K_d) for Mg^{2+} (1.7 mM) than Mn^{2+} (14 μM) (Bloom and Kameritsch, 2017). Thus, tobacco Rubisco has an affinity for each metal similar in magnitude to the activity of the metal in chloroplasts. Tobacco Rubisco, therefore, binds almost equally to both metals and rapidly exchanges one metal for the other (Bloom and Kameritsch, 2017).

4.4 | Modifying the leaf $[Mn^{2+}]/[Mg^{2+}]$ ratio to maintain the organic carbon to organic nitrogen balance

By the end of the century, global atmospheric CO_2 will increase from its current concentration of 421 ppm to between 450 and 1130 ppm (IPCC, 2021). Experiments on the responses of plants to rising CO_2 subject them to atmospheres containing higher than 550 ppm CO_2 (Broberg et al., 2019; Tcherkez et al., 2020), a concentration that is 40% above the current ambient concentration. Such treatments accelerate carbon fixation, inhibit photorespiration (Cousins and Bloom, 2004), decrease protein concentrations by over 6% (Medek et al., 2017; Myers et al., 2014; Taub et al., 2008), and increase plant C/N ratios by 20% (Butterly et al., 2015; Krämer et al., 2022; Sardans et al., 2012; Wang et al., 2019; Ziska et al., 2016).

However, atmospheric CO_2 concentrations above 550 ppm are higher than plants have experienced in more than 14 million years (Rae et al., 2021), double what plants experienced before the Industrial Revolution (Dlugokencky and Tans, 2021), and higher than what plants will experience in the next 20 years (IPCC, 2021). When exposed to less severe CO_2 enrichments, plants allocate more carbon fixation to protein synthesis and less to carbohydrate accumulation (Broberg et al., 2017; Tcherkez et al., 2020; Yang et al., 2023). For example, wheat grain yields in Californian field trials over the past 35 years declined by 13% while atmospheric CO_2 increased by 19% and grain protein concentrations remained constant (Bloom and Plant, 2021). These observations suggest that most plants maintain an organic carbon to organic nitrogen balance (i.e., C/N homeostasis) under the atmospheric CO_2 fluctuations that they experience daily, seasonally, and over decades or millennia (Nunes-Nesi et al., 2010).

The ratio of Mn^{2+} contents to Mg^{2+} contents in wheat leaves increased as atmospheric CO_2 increased and when wheat plants received NO_3^- rather than NH_4^+ as a nitrogen source (Figure S4 and Table S8). Such a shift in $[Mn^{2+}]/[Mg^{2+}]$ will enhance Rubisco oxygenation and inhibit Rubisco carboxylation, promote photorespiration and shoot NO_3^- assimilation and limit carbon assimilation, and achieve C/N homeostasis under rising atmospheric CO_2 (Bloom and Kameritsch, 2017; Bloom and Lancaster, 2018).

A recent review of photosynthetic carbon metabolism highlights the "pyruvate paradox" whereby ^{13}C only slowly appears in pyruvate after leaves are exposed to $^{13}CO_2$ (Sharkey, 2024). The author declares that one of the key issues remaining about plant carbon fixation is "The ability of Rubisco to make pyruvate has been reported once, but needs to be independently verified, and then, the consequences of this pyruvate production need additional study" (Sharkey, 2024). The results presented here directly address this issue. Conditions that favored RuBP oxygenation stimulated Rubisco generation of pyruvate from RuBP to comprise as much as 15% of the total RuBP consumed, and a substantial portion of this pyruvate may be converted into malate, as much 5% of chloroplast electron transport (Fridlyand et al., 1998).

5 | CONCLUSIONS

In summary, photorespiration is less wasteful than previously assumed because RuBP oxygenation in C_3 plants generates a substantial amount of malate in mesophyll chloroplasts through the sequential actions of Rubisco and malic enzyme. Compared to nucleoside triphosphates or reductants such as NAD(P)H and glutathione, malate is relatively stable in that it withstands storage in organelles at relatively high concentrations (>0.1 M) and rapid transport across membranes. The ubiquity of malate dehydrogenase and malic enzyme allows the generation of NADH or NADPH from malate when and where needed (Selinski and Scheibe 2019). Thus, translocating malate between organelles, cells, and tissues is a primary method through which plants and other organisms maintain redox potential in various compartments under the environmental fluctuations that occur daily, seasonally, over decades and millennia.

AUTHOR CONTRIBUTIONS

A.J.B. planned the research, obtained the funding, wrote the manuscript, and drew the figures and tables. X.S. developed the biochemical methods, edited the manuscript, and conducted experiments. N.M.H. also conducted experiments, performed the statistical analyses, and edited the manuscript.

ACKNOWLEDGMENTS

NSF grant CHE-19-04535 funded a portion of this research. We thank Professor Diane Beckles for her comments on this study.

DATA AVAILABILITY STATEMENT

Data used in this work have been uploaded to Dryad and will be made public upon publication.

ORCID

Arnold J. Bloom https://orcid.org/0000-0001-6006-1495

REFERENCES

Abadie C, Lalande J, Limami AM, Tcherkez G (2021) Non-targeted ^{13}C metabolite analysis demonstrates broad re-orchestration of leaf metabolism when gas exchange conditions vary. *Plant Cell Environ* 44: 445–457.

Alseekh S, Aharoni A, Brotman Y, Contrepois K, D'Auria J, Ewald J, C. Ewald J, Fraser PD, Giavalisco P, Hall RD, Heinemann M, Link H, Luo J, Neumann S, Nielsen J, Perez de Souza L, Saito K, Sauer U, Schroeder FC, Schuster S, Siuzdak G, Skirycz A, Sumner LW, Snyder MP, Tang H, Tohge T, Wang Y, Wen W, Wu S, Xu G, Zamboni N, Fernie AR (2021) Mass spectrometry-based metabolomics: a guide for annotation, quantification and best reporting practices. *Nature Methods* 18:747–756.

Andrews TJ, Kane HJ (1991) Pyruvate is a by-product of catalysis by ribulosebisphosphate carboxylase/oxygenase. *J Biol Chem* 266:9447–9452.

Arrivault S, Guenther M, Ivakov A, Feil R, Vosloh D, Van Dongen JT, Sulpice R, Stitt M (2009) Use of reverse-phase liquid chromatography, linked to tandem mass spectrometry, to profile the Calvin cycle and other metabolic intermediates in Arabidopsis rosettes at different carbon dioxide concentrations. *The Plant Journal* 59:826–839.

Badger MR, Andrews TJ (1974) Effects of CO_2, O_2 and temperature on a high-affinity form of ribulose diphosphate carboxylase-oxygenase from spinach. *Biochem Biophys Res Comm* 60:204–210.

Bar-On YM, Milo R (2019) The global mass and average rate of Rubisco. *Proc Nat Acad Sci USA* 116:4738–4743.

Bassham JA, Benson AA, Calvin M (1950) The path of carbon in photosynthesis: VIII. The role of malic acid. *J Biol Chem* 185:781–787.

Bathellier C, Yu L-J, Farquhar GD, Coote ML, Lorimer GH, Tcherkez G (2020) Ribulose 1,5-bisphosphate carboxylase/oxygenase activates O_2 by electron transfer. *Proc Nat Acad Sci USA* 117:24234–24242.

Beleznai Z, Szalay L, Jancsik V (1988) Ca^{2+} and Mg^{2+} as modulators of mitochondrial l-glycerol-3-phosphate dehydrogenase. *Euro J Biochem* 170:631–636.

Benson AA, Kawauchi S, Hayes P, Calvin M (1952) The path of carbon in photosynthesis. XVI. Kinetic relationships of the intermediates in steady state photosynthesis. *J Am Chem Soc* 74:4477–4482.

Bentzon-Tilia M, Severin I, Hansen LH, Riemann L (2015) Genomics and ecophysiology of heterotrophic nitrogen-fixing bacteria isolated from estuarine surface water. *MBio* 6:e00929-00915.

BioAssay Systems (2022) *EnzyChrom™ Pyruvate Assay Kit*, Hayward, CA. p^pp.

Bittig HC, Körtzinger A, Neill C, van Ooijen E, Plant JN, Hahn J, Johnson KS, Yang B, Emerson SR (2018) Oxygen optode sensors: Principle, characterization, calibration, and application in the ocean. *Front Marine Sci* 4:429.

Bloom AJ, Kameritsch P (2017) Relative association of Rubisco with manganese and magnesium as a regulatory mechanism in plants. *Physiol Plant* 161:545–559.

Bloom AJ, Lancaster KM (2018) Manganese binding to Rubisco could drive a photorespiratory pathway that increases the energy efficiency of photosynthesis. *Nature Plants* 4:414–422.

Bloom AJ, Plant RE (2021) Wheat grain yield decreased over the past 35 years, but protein content did not change. *J Exp Bot* 72:6811–6821.

Boyd RA, Cavanagh AP, Kubien DS, Cousins AB (2019) Temperature response of Rubisco kinetics in *Arabidopsis thaliana*: thermal breakpoints and implications for reaction mechanisms. *J Exp Bot* 70:231–242.

Broberg M, Högy P, Pleijel H (2017) CO_2-induced changes in wheat grain composition: Meta-analysis and response functions. *Agronomy* 7:32.

Broberg MC, Högy P, Feng Z, Pleijel H (2019) Effects of elevated CO_2 on wheat yield: Non-linear response and relation to site productivity. *Agronomy* 9:243.

Brown DA, Cook RA (1981) Role of metal cofactors in enzyme regulation. Differences in the regulatory properties of the *Escherichia coli* nicotinamide adenine dinucleotide phosphate-specific malic enzyme, depending on whether magnesium ion or manganese (2+) ion serves as divalent cation. *Biochem* 20:2503–2512.

Butterly CR, Armstrong R, Chen D, Tang C (2015) Carbon and nitrogen partitioning of wheat and field pea grown with two nitrogen levels under elevated CO_2. *Plant Soil* 391:367–382.

Cannon TM, Lagarto JL, Dyer BT, Garcia E, Kelly DJ, Peters NS, Lyon AR, French PMW, Dunsby C (2021) Characterization of NADH fluorescence properties under one-photon excitation with respect to temperature, pH, and binding to lactate dehydrogenase. *OSA continuum* 4: 1610–1625.

Carlisle E, Myers SS, Raboy V, Bloom AJ (2012) The effects of inorganic nitrogen form and CO_2 concentration on wheat yield and nutrient accumulation and distribution. *Front Plant Sci* 3:195.

Carmo-Silva AE, Keys AJ, Andralojc PJ, Powers SJ, Arrabaça MC, Parry MA (2010) Rubisco activities, properties, and regulation in three different C_4 grasses under drought. *J Exp Bot* 61:2355–2366.

Chang G-G, Tong L (2003) Structure and function of malic enzymes, a new class of oxidative decarboxylases. *Biochem* 42:12721–12733.

Christeller JT (1981) The effects of bivalent cations on ribulose bisphosphate carboxylase/oxygenase. *Biochem J* 193:839–844.

Christeller JT, Laing WA (1979) Effects of manganese ions and magnesium ions on the activity of soya-bean ribulose bisphosphate carboxylase/oxygenase. *Biochem J* 183:747–750.

Chu DK, Bassham JA (1973) Activation and inhibition of ribulose 1, 5-diphosphate carboxylase by 6-phosphogluconate. *Plant Physiol* 52:373–379.

Chu DK, Bassham JA (1974) Activation of ribulose 1,5-diphosphate carboxylase by nicotinamide adenine-dinucleotide phosphate and other chloroplast metabolites. *Plant Physiol* 54:556–559.

Clark JRLC, Wolf R, Granger D, Taylor Z (1953) Continuous recording of blood oxygen tensions by polarography. *J Appl Physiol* 6:189–193.

Cousins AB, Bloom AJ (2004) Oxygen consumption during leaf nitrate assimilation in a C_3 and C_4 plant: the role of mitochondrial respiration. *Plant Cell Environ* 27:1537–1545.

Dlugokencky E, Tans P (2021) Trends in Atmospheric Carbon Dioxide, NOAA Global Monitoring Laboratory. p^pp.

Ellis RJ (1979) The most abundant protein in the world. *Trends Biochem Sci* 4:241–244.

Fischer M, Falke D, Pawlik T, Sawers RG (2014) Oxygen-dependent control of respiratory nitrate reduction in mycelium of *Streptomyces coelicolor* A3 (2). *J Bacteriol* 196:4152–4162.

Fischer WW, Hemp J, Johnson JE (2016) Evolution of oxygenic photosynthesis. *Annu Rev Earth Planet Sci* 44:647–683.

Flitsch D, Ladner T, Lukacs M, Büchs J (2016) Easy to use and reliable technique for online dissolved oxygen tension measurement in shake flasks using infrared fluorescent oxygen-sensitive nanoparticles. *Microb Cell Factor* 15:1–11.

Fu X, Gregory LM, Weise SE, Walker BJ (2023) Integrated flux and pool size analysis in plant central metabolism reveals unique roles of glycine and serine during photorespiration. *Nature Plants* 9:169–178.

Greinert T, Baumhove K, Sadowski G, Held C (2020) Standard Gibbs energy of metabolic reactions: IV. *Triosephosphate isomerase reaction. Biophys Chem* 258:106330.

Hagemann M, Kern R, Maurino VG, Hanson DT, Weber APM, Sage RF, Bauwe H (2016) Evolution of photorespiration from cyanobacteria to land plants, considering protein phylogenies and acquisition of carbon concentrating mechanisms. *J Exp Bot* 67:2963–2976.

Hatzfeld W-D, Dancer J, Stitt M (1990) Fructose-2, 6-bisphosphate, metabolites and 'coarse'control of pyrophosphate: fructose-6-phosphate phosphotransferase during triose-phosphate cycling in heterotrophic cell-suspension cultures of *Chenopodium rubrum*. *Planta* 180:205–211.

Helm I, Karina G, Jalukse L, Pagano T, Leito I (2018) Comparative validation of amperometric and optical analyzers of dissolved oxygen: a case study. *Environ Monit Assess* 190:1–18.

Hitchman ML (1978) *Measurement of Dissolved Oxygen*. John Wiley & Sons, New York.

Iñiguez C, Niinemets Ü, Mark K, Galmés J (2021) Analyzing the causes of method-to-method variability among Rubisco kinetic traits: from the first to the current measurements. *J Exp Bot* 72:7846–7862.

IPCC (2021) *Summary for Policymakers, in Climate Change 2021: The Physical Science Basis Contribution of Working Group I to the Sixth Assessment Report of the Intergovernmental Panel on Climate Change* (Masson-Delmotte V, Zhai P, Pirani A, Connors SL, Péan C, Berger S, Caud N, Chen Y, Goldfarb L, Gomis MI, Huang M, Leitzell K, Lonnoy E, Matthews JBR, Maycock TK, Waterfield T, Yelekçi O, Yu R and Zhou B eds), Cambridge University Press, Cambridge, In Press. p^pp.

Jordan DB, Ogren WL (1983) Species variation in kinetic properties of ribulose 1, 5-bisphosphate carboxylase/oxygenase. *Arch Biochem Biophys* 227:425–433.

Krämer K, Kepp G, Brock J, Stutz S, Heyer AG (2022) Acclimation to elevated CO_2 affects the C/N balance by reducing de novo N-assimilation. *Physiol Plant* 174:e13615.

Lew LC, Choi SB, Tan PL, Liong MT (2014) Mn^{2+} and Mg^{2+} synergistically enhanced lactic acid production by *Lactobacillus rhamnosus* FTDC 8313 via affecting different stages of the hexose monophosphate pathway. *J Appl Microbiol* 116:644–653.

Lilley RMC, Walker DA (1974) An improved spectrophotometric assay for ribulosebisphosphate carboxylase. *BBA-Enzymology* 358:226–229.

Lingappa UF, Monteverde DR, Magyar JS, Valentine JS, Fischer WW (2019) How manganese empowered life with dioxygen (and vice versa). *Free Radical Biology and Medicine* 140:113–125.

Ma F, Jazmin LJ, Young JD, Allen DK (2014) Isotopically nonstationary ^{13}C flux analysis of changes in *Arabidopsis thaliana* leaf metabolism due to high light acclimation. *Proc Nat Acad Sci USA* 111:16967–16972.

Makino A, Mae T, Ohira K (1988) Differences between wheat and rice in the enzymic properties of ribulose-1, 5-bisphosphate carboxylase/oxygenase and the relationship to photosynthetic gas exchange. *Planta* 174:30–38.

Martin MN, Tabita FR (1981) Differences in the kinetic properties of the carboxylase and oxygenase activities of ribulose bisphosphate carboxylase/oxygenase. *FEBS Lett* 129:39–43.

Matsumura H, Mizohata E, Ishida H, Kogami A, Ueno T, Makino A, Inoue T, Yokota A, Mae T, Kai Y (2012) Crystal structure of rice Rubisco and implications for activation induced by positive effectors NADPH and 6-phosphogluconate. *J Molec Biol* 422:75–86.

Medek DE, Schwartz J, Myers SS (2017) Estimated effects of future atmospheric CO_2 concentrations on protein intake and the risk of protein deficiency by country and region. *Environmental Health Perspectives* 125:0870021–0870028.

Miniaev M, Belyakova M, Kostiuk N, Leshchenko D, Fedotova T (2013) Non-obvious problems in Clark electrode application at elevated temperature and ways of their elimination. *J Analyt Meth Chem* 2013.

Müller GL, Drincovich MF, Andreo CS, Lara MV (2008) *Nicotiana tabacum* NADP-malic enzyme: cloning, characterization and analysis of biological role. *Plant and cell physiology* 49:469–480.

Myers SS, Zanobetti A, Kloog I, Huybers P, Leakey ADB, Bloom AJ, Carlisle E, Dietterich LH, Fitzgerald G, Hasegawa T, Holbrook NM, Nelson RL, Ottman MJ, Raboy V, Sakai H, Sartor KA, Schwartz J, Seneweera S, Tausz M, Usui Y (2014) Increasing CO_2 threatens human nutrition. *Nature* 510:139–142.

Nunes-Nesi A, Fernie AR, Stitt M (2010) Metabolic and signaling aspects underpinning the regulation of plant carbon nitrogen interactions. *Molecular Plant* 3:973–996.

Ortner A, Huber D, Haske-Cornelius O, Weber HK, Hofer K, Bauer W, Nyanhongo GS, Guebitz GM (2015) Laccase mediated oxidation of industrial lignins: Is oxygen limiting? *Process Biochem* 50:1277–1283.

Parry MAJ, Keys AJ, Madgwick PJ, Carmo-Silva AE, Andralojc PJ (2008) Rubisco regulation: a role for inhibitors. *J Exp Bot* 59:1569–1580.

Pouvreau L, Strampraad M, Van Berloo S, Kattenberg J, de Vries S (2008) NO, N_2O, and O_2 reaction kinetics: scope and limitations of the Clark electrode. *Meth Enzymol* 436:97–112.

Rae JWB, Zhang YG, Liu X, Foster GL, Stoll HM, Whiteford RDM (2021) Atmospheric CO_2 over the Past 66 Million Years from Marine Archives. *Annu Rev Earth Planet Sci* 49:609–641.

Raverdy S, Zhang Y, Foster J, Carlow CKS (2007) Molecular and biochemical characterization of nematode cofactor independent phosphoglycerate mutases. *Molec Biochem Parasit* 156:210–216.

Sardans J, Rivas-Ubach A, Peñuelas J (2012) The C: N: P stoichiometry of organisms and ecosystems in a changing world: a review and perspectives. *Perspectives in Plant Ecology, Evolution and Systematics* 14:33–47.

Segura-Broncano L, Pukacz KR, Reichel-Deland V, Schlüter U, Triesch S, Weber APM (2023) Photorespiration is the solution, not the problem. *J Plant Physiol* 282:153928.

Selinski J, Scheibe R (2019) Malate valves: old shuttles with new perspectives. *Plant Biol* 21:21–30.

Severinghaus JW, Astrup PB (1986) History of blood gas analysis. IV. Leland Clark's oxygen electrode. *J Clinic Monit* 2:125–139.

Sharkey TD (2024) The end game(s) of photosynthetic carbon metabolism. Plant Physiol Jan 2:kiad601.

Sharkey TD, Savitch LV, Butz ND (1991) Photometric method for routine determination of k_{cat} and carbamylation of Rubisco. *Photosynth Res* 28:41–48.

Sharkey TD, Weise SE (2016) The glucose 6-phosphate shunt around the Calvin–Benson cycle. *J Exp Bot* 67:4067–4077.

Sharwood RE, Ghannoum O, Kapralov MV, Gunn LH, Whitney SM (2016) Temperature responses of Rubisco from Paniceae grasses provide opportunities for improving C_3 photosynthesis. *Nature Plants* 2:16186.

Shi X, Bloom AJ (2021) Photorespiration: The Futile Cycle? *Plants* 10:908.

Szecowka M, Heise R, Tohge T, Nunes-Nesi A, Vosloh D, Huege J, Feil R, Lunn J, Nikoloski Z, Stitt M, Fernie AR, Arrivault S (2013) Metabolic fluxes in an illuminated *Arabidopsis* rosette *The Plant Cell* 25:694–714.

Tarakhovskaya E, Marcillo A, Davis C, Milkovska-Stamenova S, Hutschenreuther A, Birkemeyer C (2023) *Matrix Effects in GC-MS Profiling of Common Metabolites after Trimethylsilyl Derivatization. Molecules 28*.

Taub DR, Miller B, Allen H (2008) Effects of elevated CO_2 on the protein concentration of food crops: a meta-analysis. *Global Change Biol* 14: 565–575.

Tcherkez G, Ben Mariem S, Larraya L, García-Mina JM, Zamarreño AM, Paradela A, Cui J, Badeck F-W, Meza D, Rizza F, Bunce J, Han X, Tausz-Posch S, Cattivelli L, Fangmeier A, Aranjuelo I (2020) Elevated CO_2 has concurrent effects on leaf and grain metabolism but minimal effects on yield in wheat. *J Exp Bot* 71:5990–5600.

Treves H, Küken A, Arrivault S, Ishihara H, Hoppe I, Erban A, Höhne M, Moraes TA, Kopka J, Szymanski J, Nikoloski Z, Stitt M (2022) Carbon flux through photosynthesis and central carbon metabolism show distinct patterns between algae, C_3 and C_4 plants. *Nature Plants* 8:78–91.

Varga A, Palmai Z, Gugolya Zn, Gráczer Ev, Vonderviszt F, Závodszky Pt, Balog E, Vas Mr (2012) Importance of aspartate residues in balancing the flexibility and fine-tuning the catalysis of human 3-phosphoglycerate kinase. *Biochem* 51:10197–10207.

Wang J, Liu X, Zhang X, Li L, Lam SK, Pan G (2019) Changes in plant C, N and P ratios under elevated [CO_2] and canopy warming in a rice-winter wheat rotation system. *Scientific Reports* 9:1–9.

Wheeler MCG, Arias CL, Tronconi MA, Maurino VG, Andreo CS, Drincovich MF (2008) *Arabidopsis thaliana* NADP-malic enzyme isoforms: high degree of identity but clearly distinct properties. *Plant Mol-Biol* 67:231–242.

Wheeler MCG, Tronconi MA, Drincovich MF, Andreo CS, Flügge U-I, Maurino VG (2005) A comprehensive analysis of the NADP-malic enzyme gene family of Arabidopsis. *Plant Physiol* 139:39–51.

Wildner GF, Henkel J (1979) The effect of divalent metal ions on the activity of Mg^{++} depleted ribulose-1, 5-bisphosphate oxygenase. *Planta* 146:223–228.

Wingfield P (1998) Protein precipitation using ammonium sulfate. Current protocols in protein science 13:A. 3F. 1-A. 3F. 8.

Wolfbeis OS (2015) Luminescent sensing and imaging of oxygen: Fierce competition to the Clark electrode. *BioEssays* 37:921–928.

Xu Y, Wieloch T, Kaste JAM, Shachar-Hill Y, Sharkey TD (2022) Reimport of carbon from cytosolic and vacuolar sugar pools into the Calvin–Benson cycle explains photosynthesis labeling anomalies. *Proc Nat Acad Sci USA* 119:e2121531119.

Yang K, Huang Y, Lv C, Yang J, Yu L, Hu Z, Sun W, Zhang Q (2023) Does elevated CO_2 cause human malnutrition? A new understanding from small and slow CO_2 change across generations in rice grain quality. *Environ Exp Bot* 208:105236.

Yokota A, Higashioka M, Wadano A (1992) Regulation of the activity of ribulose-1, 5-bisphosphate carboxylase/oxygenase through cooperative binding of 6-phosphogluconate to its regulatory sites. *Euro J Biochem* 208:721–727.

Zhang Y, Foster JM, Kumar S, Fougere M, Carlow CK (2004) Cofactor-independent phosphoglycerate mutase has an essential role in *Caenorhabditis elegans* and is conserved in parasitic nematodes. *J Biol Chem* 279:37185–37190.

Zhu A, Romero R, Petty HR (2010) A sensitive fluorimetric assay for pyruvate. *Anal Biochem* 396:146–151.

Ziska LH, Pettis JS, Edwards J, Hancock JE, Tomecek MB, Clark A, Dukes JS, Loladze I, Polley HW (2016) Rising atmospheric CO_2 is reducing the protein concentration of a floral pollen source essential for North American bees. *Proc R Soc B: Biol Sci* 283: 20160414.

SUPPORTING INFORMATION

Additional supporting information can be found online in the Supporting Information section at the end of this article.

How to cite this article: Shi, X., Hannon, N.M. & Bloom, A.J. (2024) Metals and other ligands balance carbon fixation and photorespiration in chloroplasts. *Physiologia Plantarum*, 176(4), e14463. Available from: https://doi.org/10.1111/ppl.14463